



Dynamical effects of calcium-sensitive potassium currents on voltage and calcium alternans

Matthew Kennedy² , Donald M. Bers¹ , Nipavan Chiamvimonvat^{3,4}  and Daisuke Sato¹ 

¹Department of Pharmacology, University of California, Davis, CA, USA

²Department of Biomedical Engineering, University of California, Davis, CA, USA

³Division of Cardiovascular Medicine, Department of Internal Medicine, University of California, Davis, CA, USA

⁴Department of Veterans Affairs, Northern California Health Care System, Mather, CA, USA

Key points

- A mathematical model of a small conductance Ca^{2+} -activated potassium (SK) channel was developed and incorporated into a physiologically detailed ventricular myocyte model.
- Ca^{2+} -sensitive K^+ currents promote negative intracellular Ca^{2+} to membrane voltage ($\text{Ca}_i^{2+} \rightarrow V_m$) coupling.
- Increase of Ca^{2+} -sensitive K^+ currents can be responsible for electromechanically discordant alternans and quasiperiodic oscillations at the cellular level.
- At the tissue level, Turing-type instability can occur when Ca^{2+} -sensitive K^+ currents are increased.

Abstract Cardiac alternans is a precursor to life-threatening arrhythmias. Alternans can be caused by instability of the membrane voltage (V_m), instability of the intracellular Ca^{2+} (Ca_i^{2+}) cycling, or both. V_m dynamics and Ca_i^{2+} dynamics are coupled via Ca^{2+} -sensitive currents. In cardiac myocytes, there are several Ca^{2+} -sensitive potassium (K^+) currents such as the slowly activating delayed rectifier current (I_{Ks}) and the small conductance Ca^{2+} -activated potassium (SK) current (I_{SK}). However, the role of these currents in the development of arrhythmias is not well understood. In this study, we investigated how these currents affect voltage and Ca^{2+} alternans using a physiologically detailed computational model of the ventricular myocyte and mathematical analysis. We define the coupling between V_m and Ca_i^{2+} cycling dynamics ($\text{Ca}_i^{2+} \rightarrow V_m$ coupling) as positive (negative) when a larger Ca^{2+} transient at a given beat prolongs (shortens) the action potential duration (APD) of that beat. While positive coupling predominates at baseline, increasing I_{Ks} and I_{SK} promote negative $\text{Ca}_i^{2+} \rightarrow V_m$ coupling at the cellular level. Specifically, when alternans is Ca^{2+} -driven, electromechanically (APD– Ca^{2+}) concordant alternans becomes electromechanically discordant alternans as I_{Ks} or I_{SK} increase. These cellular level dynamics lead to different types of spatially discordant alternans in tissue. These findings help to shed light on the underlying mechanisms of cardiac alternans especially when the relative strength of these currents becomes larger under pathological conditions or drug administrations.

(Resubmitted 13 October 2016; accepted after revision 22 November 2016; first published online 30 November 2016)

Corresponding author D. Sato: Department of Pharmacology, University of California, Davis, CA, USA. Email: dsato@ucdavis.edu

Abbreviations AP, action potential; APD, action potential duration; Ca_i^{2+} , intracellular Ca^{2+} ; DI, diastolic interval; g_{ks} , slowly activating delayed rectifier conductance; g_{sk} , small conductance Ca^{2+} -activated potassium conductance; I_{Ks} , slowly activating delayed rectifier current; I_{CaL} , L-type Ca^{2+} current; I_{SK} , small conductance Ca^{2+} -activated potassium current; NCX, Na^+ – Ca^{2+} exchanger; PCL, pacing cycle length; SR, sarcoplasmic reticulum; V_m , membrane voltage.

Introduction

Ventricular arrhythmia is a major cause of sudden cardiac death. It has been shown that a precursor to life-threatening arrhythmia formation is the development of cardiac alternans, a sequence of paired long and short action potentials (APs) (Pastore *et al.* 1999; Garfinkel *et al.* 2000; Fox *et al.* 2002b; Hayashi *et al.* 2007; Groenendaal *et al.* 2014). However, physiological and dynamical mechanisms are not fully understood (Weiss *et al.* 2006, 2011; Wilson *et al.* 2006; Laurita & Rosenbaum, 2008; Merchant & Armoundas, 2012; Sato & Clancy, 2013; Kanaporis & Blatter, 2015; Valdivia, 2015). At the cellular level, alternans can be caused by instability of membrane voltage (V_m) due to steep action potential duration (APD) restitution (Nolasco & Dahlen, 1968; Hayashi *et al.* 2007), instability of intracellular calcium (Ca_i^{2+}) cycling due to steep sarcoplasmic reticulum (SR) Ca^{2+} release dependence on Ca^{2+} load/refractoriness, or both (Chudin *et al.* 1999; Shiferaw *et al.* 2003, 2005; Picht *et al.* 2006; Groenendaal *et al.* 2014; Wang *et al.* 2014). Dynamical systems of V_m and Ca_i^{2+} are coupled via Ca^{2+} -sensitive currents. We previously investigated the role of the major Ca^{2+} -sensitive currents, the L-type Ca^{2+} current (I_{CaL}) and sodium(Na^+)– Ca^{2+} exchanger (NCX) (Shiferaw *et al.* 2005; Sato *et al.* 2006, 2007, 2013). However, the slowly activating delayed rectifier current (I_{Ks}) is a Ca^{2+} -sensitive current, and recent experimental studies showed that the small conductance Ca^{2+} -activated potassium (SK) channels exist in cardiac myocytes and play an important role in regulating APs (Xu *et al.* 2002; Tuteja *et al.* 2005; Zhang *et al.* 2008; Li *et al.* 2009; Hsueh *et al.* 2013; Chang *et al.* 2013a; Chang & Chen, 2015; Yu *et al.* 2015; Zhang *et al.* 2015). Yet, little is known about the role of these Ca^{2+} -sensitive K^+ currents in the formation of alternans. In this study, we investigate dynamical effects of Ca^{2+} -sensitive K^+ currents on V_m and Ca_i^{2+} alternans and show how ion channel/current level modifications lead to various phenomena at cellular and tissue levels including electromechanically (APD– Ca^{2+}) discordant alternans and spatially discordant alternans.

Methods

In order to investigate the dynamical and physiological mechanisms of alternans, we used a physiologically detailed mathematical model of AP and Ca_i^{2+} cycling of the ventricular myocyte developed by Shiferaw *et al.* (2005). Figure 1A shows the schematic diagram of the currents and fluxes that regulate V_m dynamics and Ca_i^{2+} cycling. The membrane potential is governed by

$$\frac{dV_m}{dt} = -\frac{\sum I}{C_m},$$

where V_m is the membrane potential, C_m is the cell capacitance and I represents the transmembrane currents. The details of the model are described in the online Supporting information, Data S1.

The formula of the Ca^{2+} dependence of I_{Ks} from Mahajan *et al.* (2008) was incorporated into this model. I_{Ks} is given by

$$I_{Ks} = g_{ks} x_{s1} x_{s2} q_{Ks} (V_m - E_{Ks}),$$

$$q_{Ks} = 1 + \frac{0.8}{1 + \left(\frac{K_m}{c_s}\right)^3},$$

where g_{ks} is the maximum conductance of I_{Ks} , q_{Ks} is the Ca^{2+} dependence, x_{s1} and x_{s2} are the time-dependent gating variables, E_{Ks} is the reversal potential of I_{Ks} , and K_m controls the affinity of Ca^{2+} . We varied g_{Ks} and K_m to explore the effects of I_{Ks} on alternans.

The SK channel has been recently described in atrial and ventricular myocytes (Xu *et al.* 2002; Tuteja *et al.* 2005; Zhang *et al.* 2008; Li *et al.* 2009; Hsueh *et al.* 2013; Chang *et al.* 2013a; Chang & Chen, 2015; Yu *et al.* 2015; Zhang *et al.* 2015). In this study we develop a novel computational model of the SK channel and integrate it with a physiologically detailed ionic model of a ventricular myocyte. We used the Ca^{2+} dependence formulation by Hirschberg *et al.* (1998). The governing equations for the SK channel are

$$I_{SK} = g_{sk} x_{sk} (V_m - E_K)$$

$$x_{sk} = \frac{x_{sk\infty} - x_{sk}}{\tau_{sk}}$$

$$x_{sk\infty} = 0.81 \frac{c_s^n}{c_s^n - EC_{50}^n}$$

$$\tau_{sk} = \frac{1.0}{(0.047c_s + \frac{1}{76})}$$

where g_{sk} is the maximum conductance, E_K is the reversal potential, and EC_{50} controls the affinity of Ca^{2+} . Several experimental studies have reported the EC_{50} of the SK channel in cardiac cells. Hongyuan *et al.* have reported that the EC_{50} of the SK channel in rat ventricles is 0.23–0.59 μM (Hongyuan *et al.* 2016). Chang *et al.* have reported that the EC_{50} of the SK channel in human ventricles is 0.35–0.6 μM (Chang *et al.* 2013b). In this study, we varied the EC_{50} from 0.1 to 1.0 μM to cover the whole range of physiological and pathophysiological conditions. In experimental studies, the SK current (I_{SK}) shows weak (or sometimes reverse) rectification (Lu *et al.* 2007; Zhang *et al.* 2008; Hsieh *et al.* 2013). Thus, in this study we chose a linear current–voltage relationship (Fig. 1B). Rectification properties can affect our results quantitatively. However, they did not affect our results qualitatively. Ca^{2+} dependence and its time constant are plotted in Fig. 1C and D. Figure 1E shows

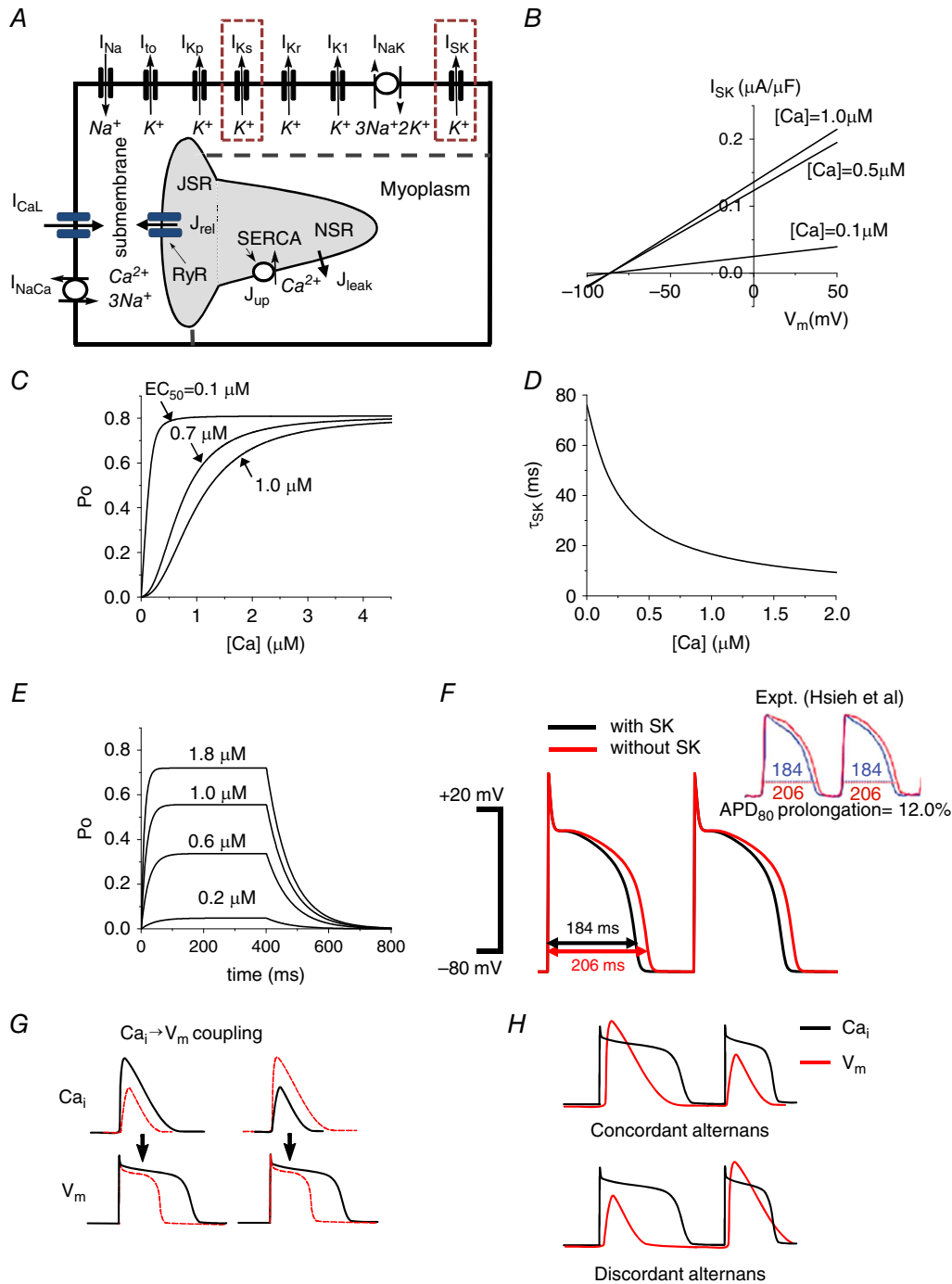


Figure 1. Physiologically detailed mathematical model
 A, schematic diagram of the currents and fluxes that regulate V_m dynamics and Ca^{2+} cycling. B, model of the SK channel: I_{SK} vs. V_m when $[Ca^{2+}]$ is 0.1, 0.5 and 1.0 μM . C, channel open probability as a function of intracellular Ca^{2+} . D, inverse relationship between intracellular Ca^{2+} and the SK time constant (τ_{SK}). E, open probability (P_o) vs. time when various test $[Ca^{2+}]$ pulses are applied. $[Ca^{2+}]$ was changed from 0 μM to test $[Ca^{2+}]$ for 400 ms, and then changed to 0 μM . F, transmembrane voltage plotted against time demonstrating the decrease in APD from baseline (red) to inclusion of the SK channel (black). When $g_{SK} = 0.8 \mu S \mu F^{-1}$ and $EC_{50} = 0.7 \mu M$ are chosen, the model shows 12% difference of APDs, which was shown by Hsieh *et al.* experimentally (Hsueh *et al.* 2013), by copyright permission of the American Heart Association, Inc. G, positive and negative $Ca_i^{2+} \rightarrow V_m$ coupling. H, electromechanically concordant (large APD \rightarrow large Ca^{2+} transient, small APD \rightarrow small Ca^{2+} transient) alternans and discordant (large APD \rightarrow small Ca^{2+} transient, small APD \rightarrow large Ca^{2+} transient) alternans.

the open probability (P_o) of the SK channel when various test $[Ca^{2+}]_i$ pulses are applied. Some reported g_{sk} values in ventricular myocytes are as high as $10 \mu S \mu F^{-1}$ (Lu *et al.* 2007; Zhang *et al.* 2008; Chang *et al.* 2013b; Hongyuan *et al.* 2016), which would profoundly shorten APD. We have chosen a range of g_{sk} more conservatively (from 0.4 to $4 \mu S \mu F^{-1}$), based on apamin effects on APD. Hsieh *et al.* showed a 12% prolongation of APD when apamin was applied (pacing cycle length, PCL = 300 ms, heart failure rabbit ventricular myocyte) (Hsueh *et al.* 2013). When g_{sk} is $0.8 \mu S \mu F^{-1}$ and EC_{50} is $0.7 \mu M$, the model also showed 12% difference between AP with I_{SK} (Fig. 1F black) and AP without I_{SK} (Fig. 1F red).

Tissue simulations were performed in a mono-domain one-dimensional cable. The governing equation for the membrane potential V_m of a cell in tissue is

$$C_m \frac{dV_m}{dt} = -I_{ion} + I_{coupling},$$

where C_m is the membrane capacitance, I_{ion} is the total ionic current through the membrane, and $I_{coupling}$ is the current that comes from the neighbouring cells through the gap junctions. This equation was solved by an operator splitting method (Qu & Garfinkel, 1999; Xie *et al.* 2004).

At the cellular level, alternans can be caused by instability of V_m due to steep APD restitution. We call this V_m -driven alternans. To alter the steepness of the restitution slope, we varied the time constant of the voltage-dependent inactivation of the L-type Ca^{2+} channel (τ_f) (Shiferaw *et al.* 2005). Alternans can also be caused by instability of Ca_i^{2+} cycling due to a steep SR Ca^{2+} release vs. SR Ca^{2+} load relationship and Ca^{2+} restitution properties. We call this Ca_i^{2+} -driven alternans (Chudin *et al.* 1999; Shiferaw *et al.* 2003, 2005). To alter the instability of Ca_i^{2+} cycling, we varied the gain of the SR Ca^{2+} release function (u) (Shiferaw *et al.* 2005).

Coupling of Ca^{2+} on the APD ($Ca_i^{2+} \rightarrow V_m$ coupling) is defined as positive (negative) if a large Ca^{2+} transient prolongs (shortens) the APD of the same beat (Shiferaw *et al.* 2005; Weiss *et al.* 2006) (Fig. 1G). In our previous study (Shiferaw *et al.* 2005), we controlled $Ca_i^{2+} \rightarrow V_m$ coupling with a varying relative contribution of I_{CaL} and NCX by changing the Ca^{2+} -induced inactivation strength (γ). As γ is increased, I_{CaL} dominates and $Ca_i^{2+} \rightarrow V_m$ coupling becomes more negative. The $Ca_i^{2+} \rightarrow V_m$ coupling is positive when γ is 0.7. By fixing $\gamma = 0.7$ and varying Ca^{2+} -sensitive K^+ currents, we demonstrate that Ca^{2+} -sensitive K^+ currents can change the $Ca_i^{2+} \rightarrow V_m$ coupling.

V_m and Ca_i^{2+} alternans can be electromechanically concordant (a Long–Short–Long–Short APD sequence corresponding to a Large–Small–Large–Small Ca^{2+} transient sequence) or discordant (a Long–Short–Long–Short APD sequence corresponding to a Small–Large–Small–Large Ca^{2+} transient sequence)

(Fig. 1H). These phenomena depend on the underlying instability mechanisms (V_m -driven or Ca_i^{2+} -driven) and the coupling between V_m and Ca_i^{2+} cycling.

Results

I_{SK} is an outward current during the AP. Introduction of the SK channel, while keeping all other parameters constant as in Shiferaw *et al.* (2005) was shown to shorten the APD (Fig. 1F) similar to other outward currents.

Introduction of I_{SK} increases the area of stable APs with three distinct modes of oscillations at the stability boundary

By varying the instability factors of V_m (τ_f) and Ca_i^{2+} cycling (u), we plotted the stability diagram (Fig. 2A and B) for the pacing cycle length (PCL) of 300 ms. Without I_{SK} (Fig. 2A), the $Ca_i^{2+} \rightarrow V_m$ coupling is positive and alternans was always electromechanically concordant regardless of the instability mechanism. When I_{SK} was introduced ($g_{sk} = 4 \mu S \mu F^{-1}$, $EC_{50} = 0.7 \mu M$), the area of the stable APs (i.e. periodic APs) was increased, evident from Fig. 2A and B. In addition, three distinct modes of oscillations, electromechanically concordant alternans, quasiperiodic oscillations and electromechanically discordant alternans, occurred at the stability boundary, as labelled in Fig. 2B (as C, D, E). The relation between peak $[Ca^{2+}]_i$ and APD was plotted, with (C) corresponding to electromechanically concordant alternans, (D) representing electromechanically discordant alternans as seen by the negative relation between peak $[Ca^{2+}]_i$ and APD, while (E) shows the quasiperiodic oscillation with corresponding orbit in peak $[Ca^{2+}]_i$ –APD plane (Fig. 2E right panel). From our previous study (Shiferaw *et al.* 2005) three modes of oscillations implies that the $Ca_i^{2+} \rightarrow V_m$ coupling is negative.

Affinity of $[Ca^{2+}]_i$ also affects V_m – Ca_i^{2+} dynamics

Figure 3A shows how the stability boundary curves (at PCL = 300 ms) shift with increasing I_{SK} conductance (g_{sk}). Figure 3B shows how these curves shift as the I_{SK} $[Ca^{2+}]_i$ dependence (EC_{50}) is altered from 0.1 to $1.0 \mu M$. When Ca^{2+} affinity is high (lower EC_{50}), I_{SK} shortens both short AP and long AP regardless of the amplitude of the Ca^{2+} transient. However, when Ca^{2+} affinity becomes lower (higher EC_{50}), I_{SK} shortens only when the amplitude of the Ca^{2+} transient is large. This means that the change in the APD becomes larger even when the change in the amplitude of the Ca^{2+} transient is the same. This promotes negative $Ca_i^{2+} \rightarrow V_m$ coupling (ΔAPD vs. $\Delta peak [Ca^{2+}]_i$ will become steeper).

To test this idea of coupling change, we plotted Δ APD vs. peak $[Ca^{2+}]_i$ (Fig. 3C) for small changes in $[Ca^{2+}]_i$. Peak $[Ca^{2+}]_i$ was varied by changing initial (diastolic) SR Ca²⁺ load. Without I_{SK} the positive slope indicates positive $Ca_i^{2+} \rightarrow V_m$ coupling, but as g_{sk} increases the slope flattens and by $g_{sk} = 4 \mu S \mu F^{-1}$, the $Ca_i^{2+} \rightarrow V_m$ coupling becomes substantially negative (Fig. 3C). The sign was changed around $g_{sk} = 1 \mu S \mu F^{-1}$ (Fig. 3D). Higher Ca²⁺ affinity

also makes the $Ca_i^{2+} \rightarrow V_m$ coupling more negative (Fig. 3E and F).

I_{Ks} is also Ca²⁺ sensitive. As expected, qualitatively similar results are seen with increasing I_{Ks} as were seen with I_{SK} . When the maximum conductance of I_{Ks} (g_{ks}) is reduced by half, we observed electro-mechanically concordant alternans at the stability boundaries (Fig. 4A). On the other hand, when g_{ks} is

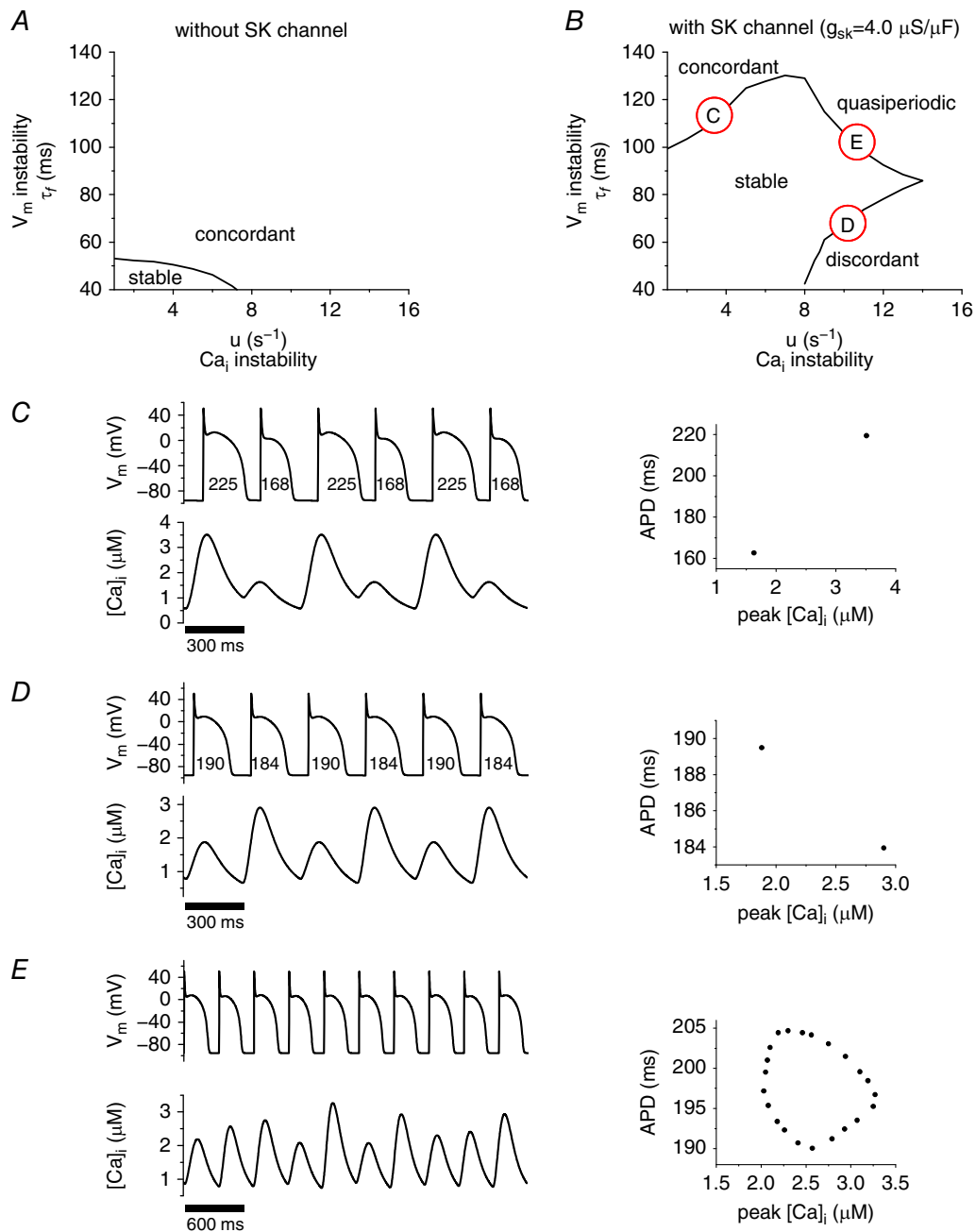


Figure 2. Effects of I_{SK} at the cellular level

Stability boundaries were numerically determined for both the baseline system and the baseline plus SK, as seen in A and B, respectively. A demonstrates one mode of instability, namely concordant alternans, while B shows three distinct modes of instability; concordant alternans (C), discordant alternans (D), and quasiperiodic oscillation (E).

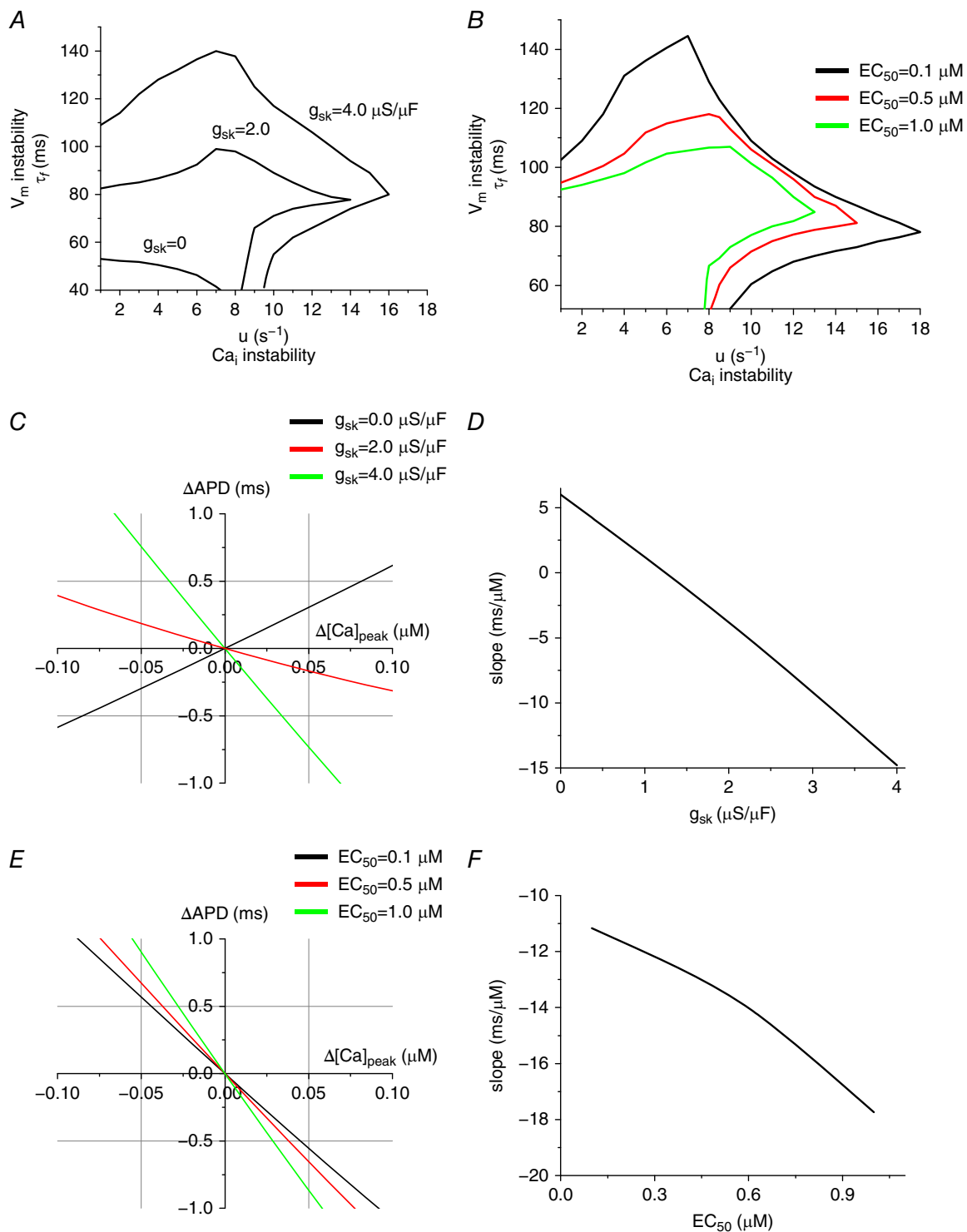


Figure 3. Effects of the maximum conductance and Ca^{2+} affinity of I_{SK}

A, stability boundaries plotted for three g_{sk} , with values of 0, 2.0 and $4.0 \mu S \mu F^{-1}$. *B*, stability boundaries plotted for three EC_{50} values of 1.0, 0.5 and $0.1 \mu M$ corresponding to the black, red and green curves, respectively. *C*, the slope of ΔAPD vs. $\Delta[Ca^{2+}]_{peak}$ indicates the $Ca_i^{2+} \rightarrow V_m$ coupling. When $g_{sk} = 0 \mu S \mu F^{-1}$, the $Ca_i^{2+} \rightarrow V_m$ coupling is positive, while when $g_{sk} = 4.0 \mu S \mu F^{-1}$, the $Ca_i^{2+} \rightarrow V_m$ coupling is negative. EC_{50} is $0.7 \mu M$. *D*, slope ($\Delta APD/\Delta[Ca^{2+}]_{peak}$) vs. g_{sk} . *E*, ΔAPD vs. $\Delta[Ca^{2+}]_{peak}$ when EC_{50} is varied. g_{sk} is $4.0 \mu S \mu F^{-1}$. *F*, slope ($\Delta APD/\Delta[Ca^{2+}]_{peak}$) vs. EC_{50} .

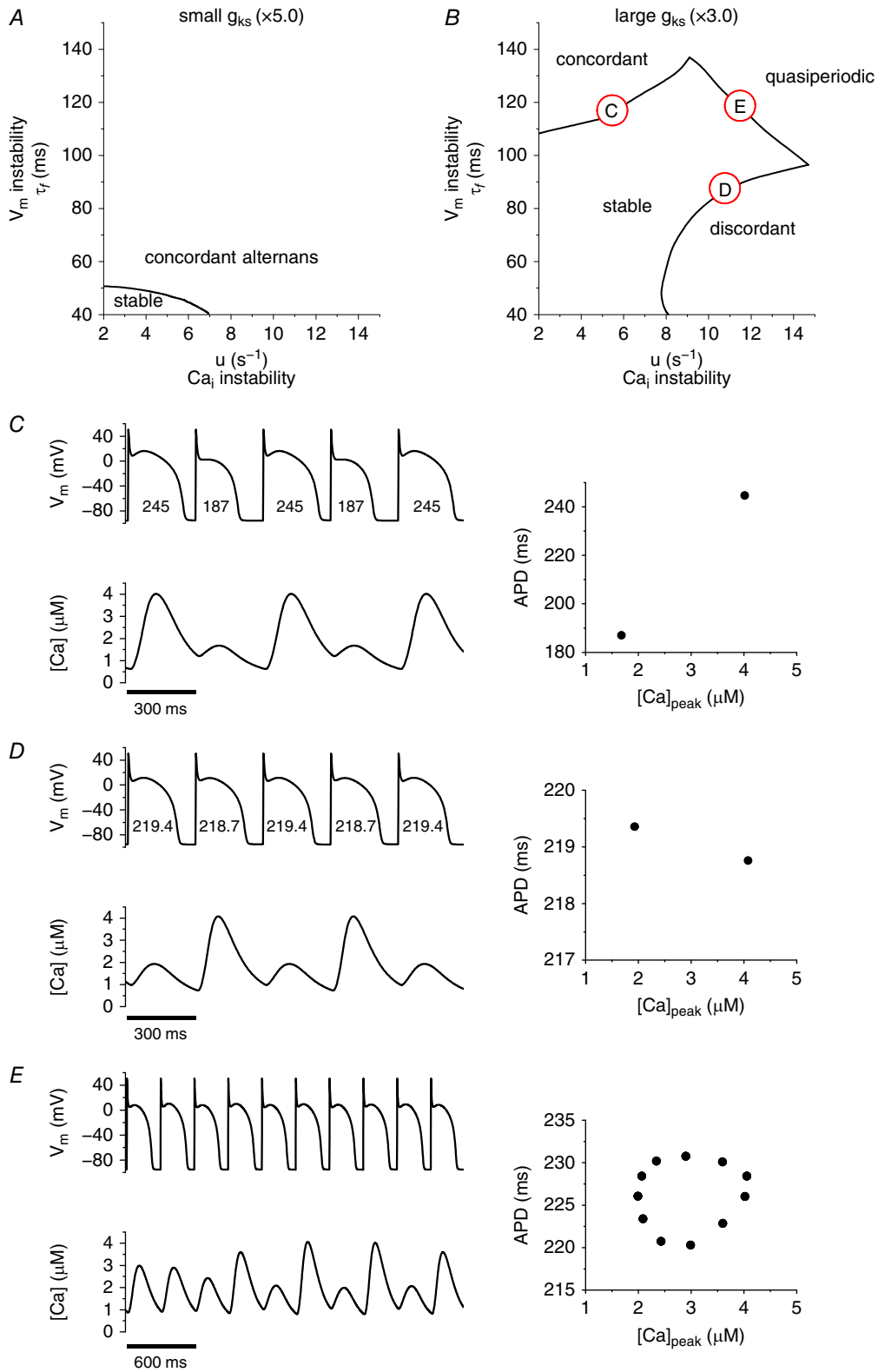


Figure 4. Effects of I_{Ks} at the cellular level

A, stability diagram when g_{Ks} is small (50% of the original value, the original g_{Ks} is $0.0245 \text{ mS } \mu\text{F}^{-1}$). Alternans is always electromechanically concordant. B, stability diagram when g_{Ks} is large (300% of the original value). In this case, there are three distinct modes of instability; electromechanically concordant alternans (C), electromechanically discordant alternans (D), and quasiperiodic oscillation (E).

increased to 300%, we observed three modes of oscillations (Fig. 4B). These modes are plotted in Fig. 4C (electro-mechanically concordant alternans), Fig. 4D (electro-mechanically discordant alternans), and Fig. 4E (quasi-periodic oscillations).

Both the maximum conductance (g_{ks}) and Ca^{2+} sensitivity affect the stability boundaries and the modes of oscillations

When g_{ks} was increased from 50 to 300%, it not only increased the stable area but also induced three modes (Fig. 5A). On the other hand, when Ca^{2+} sensitivity was

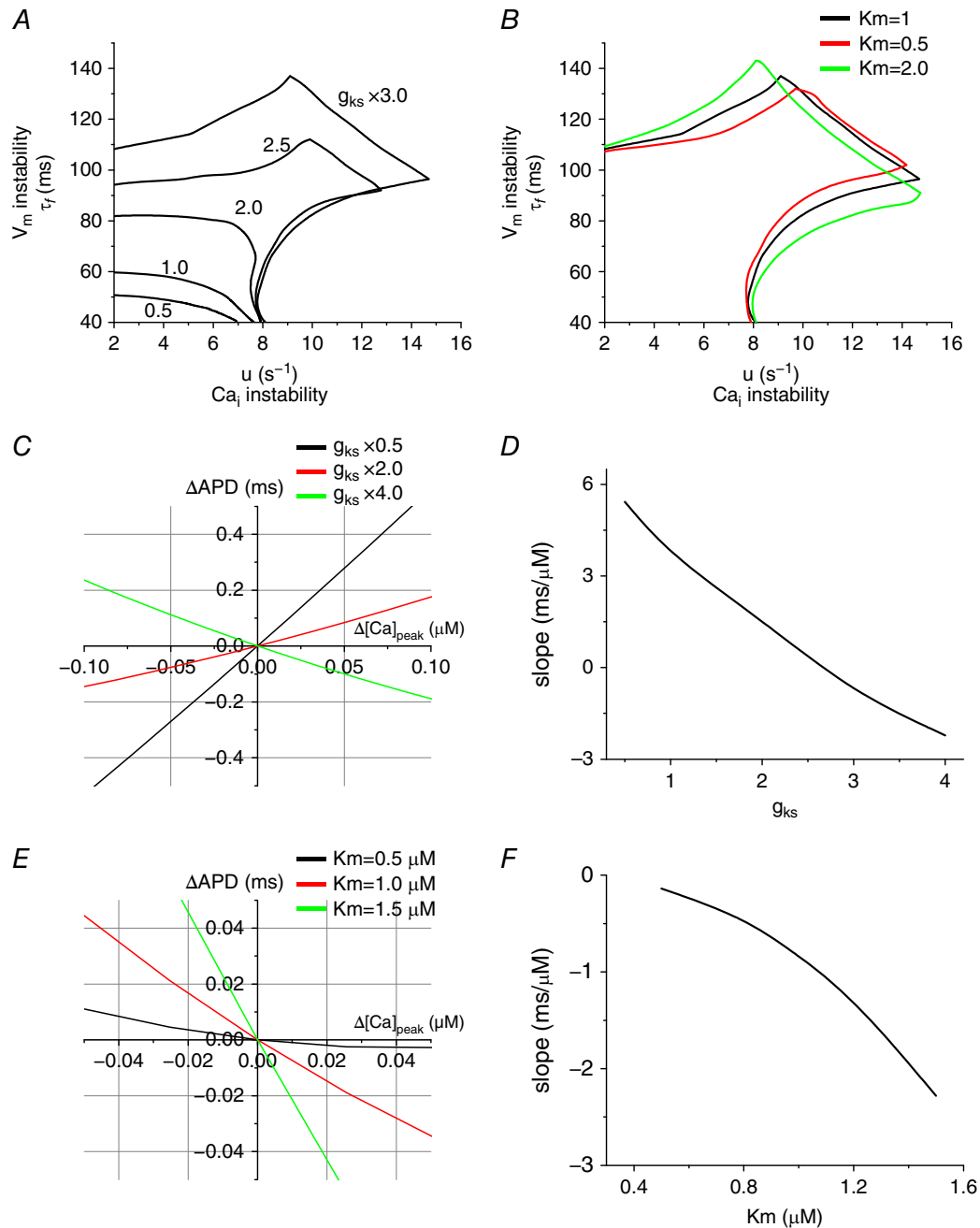


Figure 5. Effects of the maximum conductance and Ca^{2+} affinity of I_{ks}

A, stability boundaries plotted for multiple g_{ks} , with values of 50, 100, 200, 250 and 300% of the original value ($0.0245 \text{ mS } \mu F^{-1}$). B, stability boundaries plotted for three K_m , with values of 1.0, 0.5 and 2.0 μM corresponding to the black, red and green curves, respectively. C, ΔAPD vs. $\Delta [Ca^{2+}]_{peak}$ when g_{ks} is varied. D, slope ($\Delta APD/\Delta [Ca^{2+}]_{peak}$) vs. g_{ks} . E, ΔAPD vs. $\Delta [Ca^{2+}]_{peak}$ when K_m is varied. F, slope ($\Delta APD/\Delta [Ca^{2+}]_{peak}$) vs. K_m .

decreased, it suppressed electromechanically concordant and discordant alternans but promoted quasiperiodic oscillations (Fig. 5B). This indicates that Ca²⁺ sensitivity changed only the coupling without changing V_m and Ca_i²⁺ instabilities. Figure 5C and D shows positive Ca_i²⁺ → V_m coupling when I_{Ks} is small ($g_{ks} \times 0.5$) and negative Ca_i²⁺ → V_m coupling when I_{Ks} is large ($g_{ks} \times 3$).

From these single cell simulations, we summarize as follows. If alternans is Ca_i²⁺-driven (small τ_f and large u , along the abscissa in Figs 2–4), increasing the maximum conductance of I_{SK} or I_{Ks} promotes electromechanically discordant alternans (Fig. 6A). On the other hand, if alternans is V_m -driven (large τ_f and small u , along ordinate in Figs 2–4), electromechanically concordant alternans remains electromechanically concordant even when the maximum conductance of I_{SK} or I_{Ks} is increased (Fig. 6B).

At the tissue level, increasing I_{SK} or I_{Ks} leads to different types of spatially discordant alternans

In tissue, cellular level instability mechanisms lead to different alternans. We paced the left-most five cells of the 6 cm (400 cell) homogeneous cable. First, we paced the cable at a PCL of 600 ms until it reached the steady state. At this PCL, there is no alternans. Then, the PCL was decreased to 300 ms. Alternans gradually developed.

When all cells in the cable reached the steady state, we plotted APD and peak [Ca²⁺]_i along the cable (Fig. 7).

When alternans are Ca_i²⁺-driven (small τ_f and large u), if these currents are small, the Ca_i²⁺ → V_m coupling is positive and the mechanism of spatially discordant alternans is due to competition between synchronization due to diffusive electrical coupling and desynchronization due to Ca²⁺-related stochasticity (Sato *et al.* 2013). The mechanism of spatially discordant alternans does not depend on the details of the ionic currents. This occurs whenever the cellular level instability mechanism is Ca_i²⁺-driven and the Ca_i²⁺ → V_m coupling is positive. In this case, the spatial scale of phase reversal of Ca_i²⁺ alternans is short (Sato *et al.* 2007) (Fig. 7A and D), where spatially discordant alternans is shown. However, when I_{SK} or I_{Ks} becomes large, the Ca_i²⁺ → V_m coupling becomes negative and the mechanism of spatially discordant alternans is due to Turing-type instability (instability due to electrotonic coupling) (Sato *et al.* 2006) (Fig. 7B and E). The mechanism of this spatially discordant alternans is also model independent and requires only Ca_i²⁺-driven instability and negative Ca_i²⁺ → V_m coupling. If alternans is V_m -driven, the mechanism of spatially discordant alternans is due to interaction between APD and conduction velocity restitution (Echebarria & Karma, 2002, 2007) (Fig. 7C and F). In this case, the spatial scales

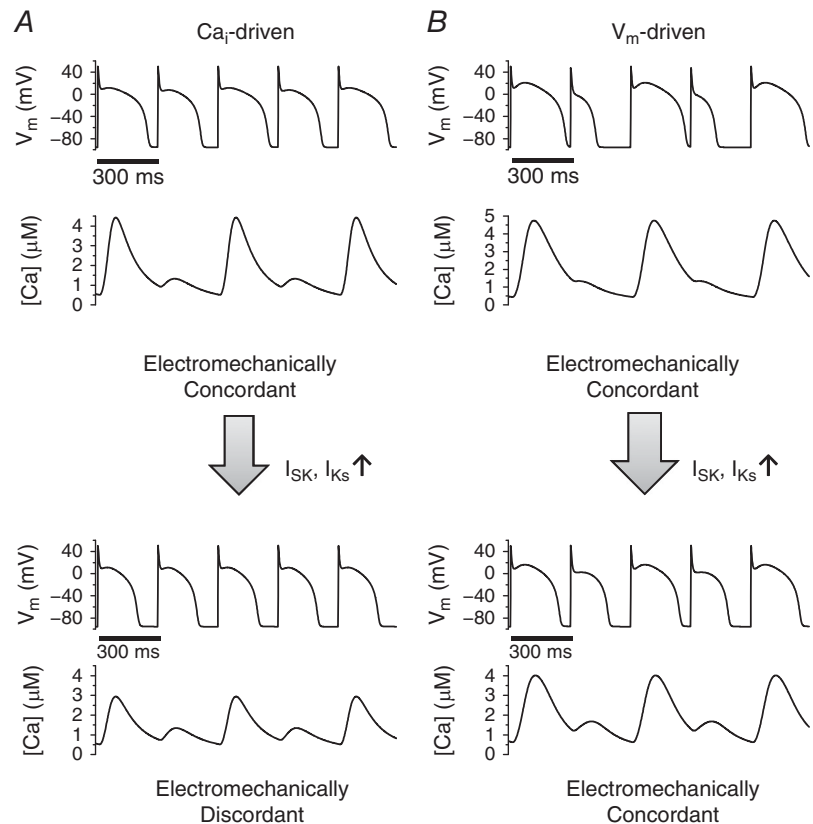


Figure 6. Summary of the effects of Ca²⁺-sensitive K⁺ currents

A, if alternans is Ca_i²⁺-driven, Ca²⁺-sensitive K⁺ currents promote electromechanically discordant alternans. B, if alternans is V_m -driven, electromechanically concordant alternans remains electromechanically concordant even when Ca²⁺-sensitive K⁺ currents are increased.

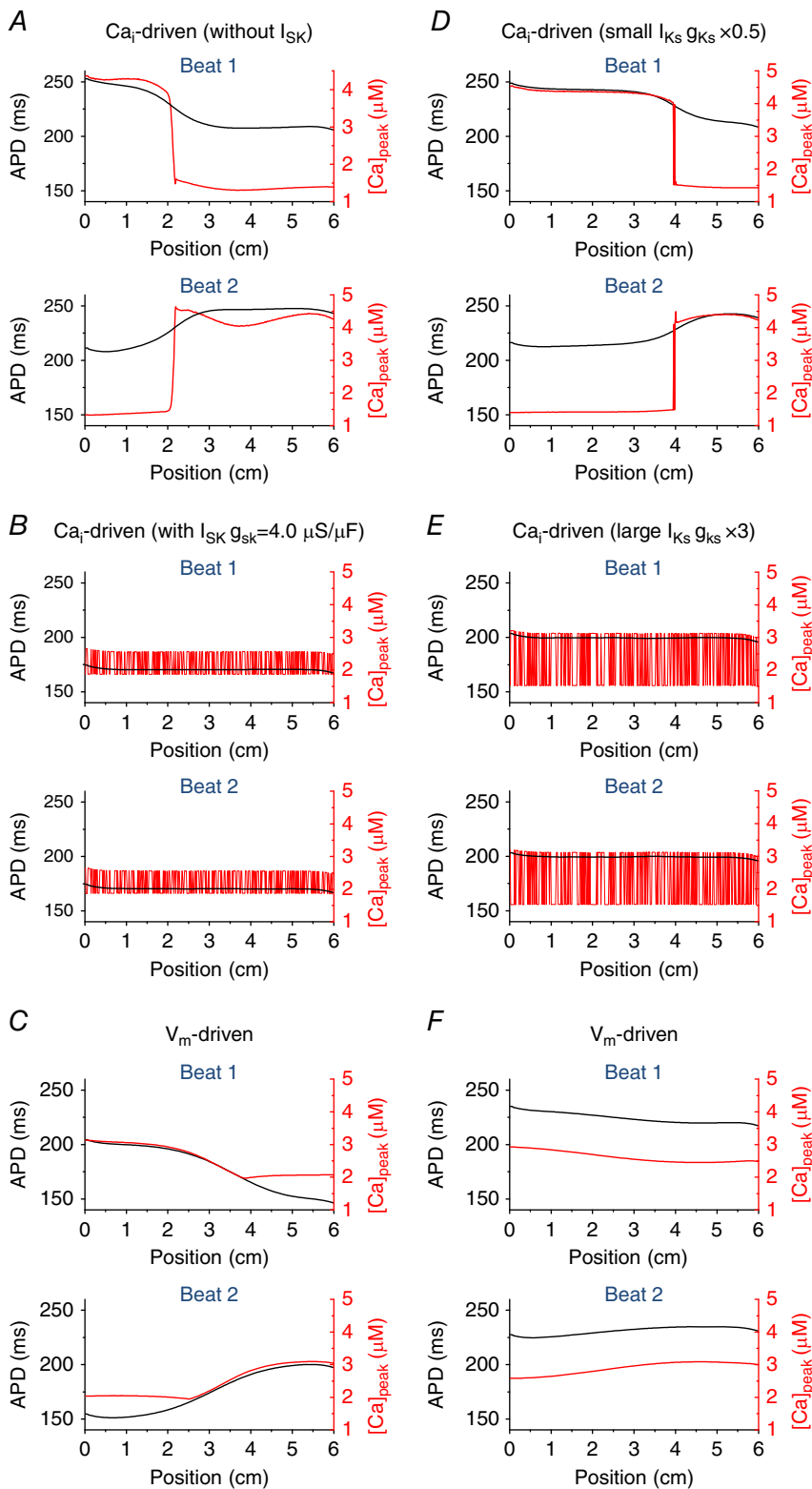


Figure 7. Effects of I_{SK} and I_{KS} at the tissue level

A, Ca^{2+} -driven alternans without I_{SK} . The mechanism of spatially discordant alternans is competition between synchronization due to diffusive coupling and desynchronization due to stochasticity. *B*, Ca^{2+} -driven alternans with I_{SK} . The mechanism of spatially discordant alternans is Turing-type instability. *C*, V_m -driven alternans. The mechanism of spatially discordant alternans is interaction between APD and conduction velocity restitution. When alternans is V_m -driven, changing the magnitude of I_{SK} does not change the mechanism of spatially discordant alternans. In this simulation, g_{SK} is $4.0 \mu\text{S} \mu\text{F}^{-1}$. *D*, Ca^{2+} -driven alternans when g_{KS} is small (50% of the original value). The mechanism of spatially discordant alternans is competition between synchronization due to diffusive coupling and desynchronization due to stochasticity. *E*, Ca^{2+} -driven alternans when g_{KS} is large (300% of the original value). The mechanism of spatially discordant alternans is Turing-type instability. *F*, V_m -driven alternans. The mechanism of spatially discordant alternans is interaction between APD and conduction velocity restitution. When alternans is V_m -driven, changing the magnitude of I_{KS} does not change the mechanism of spatially discordant alternans. In this simulation, g_{KS} is 300% of the original value.

of phase reversal of Ca_i²⁺ alternans is large (e.g. vs. that in Fig. 7A and D) (Sato *et al.* 2007).

Discussion

In this study, we have shown that Ca²⁺-sensitive K⁺ currents I_{Ks} and I_{SK} promote negative Ca_i²⁺ → V_m coupling, which creates three modes of instability at the cellular level and Turing-type instability at the tissue level.

In 1968, Nolasco and Dahlen used APD restitution, which is the relationship between APD and the previous diastolic interval (DI), $APD(n+1) = \text{Function}(F)(DI(n))$, to demonstrate that the formation of alternans occurs when the slope of the APD restitution curve exceeds unity (Nolasco & Dahlen, 1968). This interpretation provides a model for the relationship of V_m and APD stability. However, this one-dimensional map cannot explain the existence of three distinct modes (electromechanically concordant/discordant alternans and quasi-periodicity) of instability (Shiferaw *et al.* 2005), which have been shown experimentally (Rubenstein & Lipsius, 1995; Gilmour *et al.* 1997; Walker & Rosenbaum, 2003).

One possible mechanism for these multiple modes is the interactions between V_m and Ca_i²⁺ cycling. Ca_i²⁺ cycling can be unstable when the myocyte is Ca²⁺ overloaded or RyRs are sensitized. Ca_i²⁺ cycling can also be unstable when the cell is rapidly paced. In fact, Chudin *et al.* have demonstrated that Ca_i²⁺ transients exhibit alternans even with AP clamp waveform (i.e. APs are periodic) (Chudin *et al.* 1999). This implies that Ca_i²⁺ cycling has its own non-linear dynamics (Dilly & Lab, 1988; Hall *et al.* 1999; Hall & Gauthier, 2002; Fox *et al.* 2002a; Pruvot *et al.* 2004; Picht *et al.* 2006; Wang *et al.* 2014).

In the present study, we used a computational model which shows both non-linearities of V_m and Ca_i²⁺ cycling. These two non-linear systems are coupled via Ca²⁺-sensitive currents. As the myocyte experiences a large Ca²⁺ transient, the open probability of the Ca²⁺-sensitive K⁺ channel will increase, increasing outward K⁺ current. This larger Ca²⁺ transient also promotes Ca²⁺-dependent inactivation of L-type Ca²⁺ channels, limiting inward Ca²⁺ current, so both K⁺ and Ca²⁺ current effects tend to promote negative Ca_i²⁺ → V_m coupling. However, Ca²⁺-dependence increases in inward current via NCX (due to changes in electrochemical driving force) promoting positive Ca_i²⁺ → V_m coupling. Net changes in the competition between these Ca²⁺-dependent currents produces the transition from positive to negative Ca_i²⁺ → V_m coupling. Any increase in Ca²⁺-dependent K⁺ current (I_{Ks} or I_{SK}) would tend to shift the coupling negative. Moreover, increasing either I_{Ks} or I_{SK} reveals three modes of instability. As the Ca_i²⁺ → V_m coupling becomes more negative (with rising I_{Ks} or I_{SK}), the slope of ΔAPD vs. ΔCa^{2+} is negative, and three distinct modes of

alternans are induced: (1) V_m -driven electromechanically concordant alternans (large τ_f , small u), (2) Ca_i²⁺-driven electromechanically discordant alternans (small τ_f , large u), and (3) quasiperiodic oscillation (large τ_f , large u). All three of these modes of instability have been observed in both voltage and Ca²⁺ recordings (Dilly & Lab, 1988; Hall *et al.* 1999; Hall & Gauthier, 2002; Fox *et al.* 2002a; Pruvot *et al.* 2004).

Another important point of this study is that we introduced a novel model of the SK channel. Using this model, we demonstrate that its Ca²⁺ dependence (Hirschberg *et al.* 1998) is responsible for the observed existence of three distinct modes of instability.

Typical healthy myocytes show electromechanically concordant alternans during fast pacing. We found that as the maximum conductance of I_{SK} was increased, electromechanically concordant alternans became electromechanically discordant when alternans is Ca_i²⁺-driven. These findings shed light on the underlying mechanisms of cardiac alternans, especially for failing hearts since I_{SK} was shown to be up-regulated in ventricular myocytes in heart failure (Yu *et al.* 2015). In this study, we used a ventricular AP model. Alternans have also been observed in atrial cells (Kanaporis & Blatter, 2015). We expect I_{SK} to have the same dynamical effects on alternans in atrial cells, and may be even more impactful there because of higher basal density of I_{SK} in atrial vs. ventricular myocytes (Xu *et al.* 2003). Finally, our study also provides insights into the non-linearities of cardiac tissue behaviour and a potential link between molecular processes within the cell to the development of disorders of the organ itself.

References

- Chang P-C & Chen P-S (2015). SK channels and ventricular arrhythmias in heart failure. *Trends Cardiovasc Med* **25**, 508–514.
- Chang P-C, Hsieh Y-C, Hsueh C-H, Weiss JN, Lin S-F & Chen P-S (2013a). Apamin induces early afterdepolarizations and torsades de pointes ventricular arrhythmia from failing rabbit ventricles exhibiting secondary rises in intracellular calcium. *Heart Rhythm* **10**, 1516–1524.
- Chang PC, Turker I, Lopshire JC, Masroor S, Nguyen BL, Tao W, Rubart M, Chen PS, Chen Z & Ai T (2013b). Heterogeneous upregulation of apamin-sensitive potassium currents in failing human ventricles. *J Am Heart Assoc* **2**, e004713.
- Chudin E, Goldhaber J, Garfinkel A, Weiss J & Kogan B (1999). Intracellular Ca²⁺ dynamics and the stability of ventricular tachycardia. *Biophys J* **77**, 2930–2941.
- Dilly SG & Lab MJ (1988). Electrophysiological alternans and restitution during acute regional ischaemia in myocardium of anaesthetized pig. *J Physiol* **402**, 315–333.
- Echebarria B & Karma A (2002). Instability and spatiotemporal dynamics of alternans in paced cardiac tissue. *Phys Rev Lett* **88**, 208101.

- Echebarria B & Karma A (2007). Amplitude equation approach to spatiotemporal dynamics of cardiac alternans. *Phys Rev E Stat Nonlin Soft Matter Phys* **76**, 051911.
- Fox JJ, Bodenschatz E & Gilmour RF Jr (2002a). Period-doubling instability and memory in cardiac tissue. *Phys Rev Lett* **89**, 138101.
- Fox JJ, McHarg JL & Gilmour RF Jr (2002b). Ionic mechanism of electrical alternans. *Am J Physiol Heart Circ Physiol* **282**, H516–H530.
- Garfinkel A, Kim YH, Voroshilovsky O, Qu Z, Kil JR, Lee MH, Karagueuzian HS, Weiss JN & Chen PS (2000). Preventing ventricular fibrillation by flattening cardiac restitution. *Proc Natl Acad Sci USA* **97**, 6061–6066.
- Gilmour RF, Otani NF & Watanabe MA (1997). Memory and complex dynamics in cardiac Purkinje fibers. *Am J Physiol Heart Circ Physiol* **272**, H1826–H1832.
- Groenendaal W, Ortega FA, Krogh-Madsen T & Christini DJ (2014). Voltage and calcium dynamics both underlie cellular alternans in cardiac myocytes. *Biophys J* **106**, 2222–2232.
- Hall GM, Bahar S & Gauthier DJ (1999). Prevalence of rate-dependent behaviors in cardiac muscle. *Phys Rev Lett* **82**, 2995–2998.
- Hall GM & Gauthier DJ (2002). Experimental control of cardiac muscle alternans. *Phys Rev Lett* **88**, 198102.
- Hayashi H, Shiferaw Y, Sato D, Nihei M, Lin S-F, Chen P-S, Garfinkel A, Weiss JN & Qu Z (2007). Dynamic origin of spatially discordant alternans in cardiac tissue. *Biophys J* **92**, 448–460.
- Hirschberg B, Maylie J, Adelman JP & Marrion NV (1998). Gating of recombinant small-conductance Ca-activated K⁺ channels by calcium. *J Gen Physiol* **111**, 565–581.
- Hongyuan B, Xin D, Jingwen Z, Li G & Yajuan N (2016). Apamin-sensitive small conductance calcium-activated potassium channels were negatively regulated by captopril in volume-overload heart failure rats. *J Membr Biol* **249**, 429–436.
- Hsieh YC, Chang PC, Hsueh CH, Lee YS, Shen C, Weiss JN, Chen Z, Ai T, Lin SF & Chen PS (2013). Apamin-sensitive potassium current modulates action potential duration restitution and arrhythmogenesis of failing rabbit ventricles. *Circ Arrhythm Electrophysiol* **6**, 410–418.
- Hsueh C-H, Chang P-C, Hsieh Y-C, Reher T, Chen P-S & Lin S-F (2013). Proarrhythmic effect of blocking the small conductance calcium activated potassium channel in isolated canine left atrium. *Heart Rhythm* **10**, 891–898.
- Kanaporis G & Blatter LA (2015). The mechanisms of calcium cycling and action potential dynamics in cardiac alternans. *Circ Res* **116**, 846–856.
- Laurita KR & Rosenbaum DS (2008). Cellular mechanisms of arrhythmogenic cardiac alternans. *Prog Biophys Mol Biol* **97**, 332–347.
- Li N, Timofeyev V, Tuteja D, Xu D, Lu L, Zhang Q, Zhang Z, Singapuri A, Albert TR, Rajagopal AV, Bond CT, Periasamy M, Adelman J & Chiamvimonvat N (2009). Ablation of a Ca²⁺-activated K⁺ channel (SK2 channel) results in action potential prolongation in atrial myocytes and atrial fibrillation. *J Physiol* **587**, 1087–1100.
- Lu L, Zhang Q, Timofeyev V, Zhang Z, Young JN, Shin H-S, Knowlton AA & Chiamvimonvat N (2007). Molecular coupling of a Ca²⁺-activated K⁺ channel to L-type Ca²⁺ channels via α -actinin2. *Circ Res* **100**, 112–120.
- Mahajan A, Shiferaw Y, Sato D, Baher A, Olcese R, Xie LH, Yang MJ, Chen PS, Restrepo JG, Karma A, Garfinkel A, Qu Z & Weiss JN (2008). A rabbit ventricular action potential model replicating cardiac dynamics at rapid heart rates. *Biophys J* **94**, 392–410.
- Merchant FM & Armoundas AA (2012). Role of substrate and triggers in the genesis of cardiac alternans, from the myocyte to the whole heart: implications for therapy. *Circulation* **125**, 539–549.
- Nolasco JB & Dahlen RW (1968). A graphic method for the study of alternation in cardiac action potentials. *J Appl Physiol* **25**, 191–196.
- Pastore JM, Girouard SD, Laurita KR, Akar FG & Rosenbaum DS (1999). Mechanism linking T-wave alternans to the genesis of cardiac fibrillation. *Circulation* **99**, 1385–1394.
- Picht E, DeSantiago J, Blatter LA & Bers DM (2006). Cardiac alternans do not rely on diastolic sarcoplasmic reticulum calcium content fluctuations. *Circ Res* **99**, 740–748.
- Pruvot EJ, Katra RP, Rosenbaum DS & Laurita KR (2004). Role of calcium cycling versus restitution in the mechanism of repolarization alternans. *Circ Res* **94**, 1083–1090.
- Qu Z & Garfinkel A (1999). An advanced algorithm for solving partial differential equation in cardiac conduction. *IEEE Trans Biomed Eng* **46**, 1166–1168.
- Rubenstein DS & Lipsius SL (1995). Premature beats elicit a phase reversal of mechano-electrical alternans in cat ventricular myocytes: a possible mechanism for reentrant arrhythmias. *Circulation* **91**, 201–214.
- Sato D, Bers DM & Shiferaw Y (2013). Formation of spatially discordant alternans due to fluctuations and diffusion of calcium. *PLoS One* **8**, e85365.
- Sato D & Clancy CE (2013). Cardiac electrophysiological dynamics from the cellular level to the organ level. *Biomed Eng Comput Biol* **5**, 69–75.
- Sato D, Shiferaw Y, Garfinkel A, Weiss JN, Qu Z & Karma A (2006). Spatially discordant alternans in cardiac tissue: role of calcium cycling. *Circ Res* **99**, 520–527.
- Sato D, Shiferaw Y, Qu Z, Garfinkel A, Weiss JN & Karma A (2007). Inferring the cellular origin of voltage and calcium alternans from the spatial scales of phase reversal during discordant alternans. *Biophys J* **92**, L33–L35.
- Shiferaw Y, Sato D & Karma A (2005). Coupled dynamics of voltage and calcium in paced cardiac cells. *Phys Rev E Stat Nonlin Soft Matter Phys* **71**, 021903.
- Shiferaw Y, Watanabe MA, Garfinkel A, Weiss JN & Karma A (2003). Model of intracellular calcium cycling in ventricular myocytes. *Biophys J* **85**, 3666–3686.
- Tuteja D, Xu D, Timofeyev V, Lu L, Sharma D, Zhang Z, Xu Y, Nie L, Vazquez AE, Young JN, Glatzer KA & Chiamvimonvat N (2005). Differential expression of small-conductance Ca²⁺-activated K⁺ channels SK1, SK2, and SK3 in mouse atrial and ventricular myocytes. *Am J Physiol Heart Circ Physiol* **289**, H2714–H2723.

- Valdivia HH (2015). Mechanisms of cardiac alternans in atrial cells: intracellular Ca²⁺ disturbances lead the way. *Circ Res* **116**, 778–780.
- Walker ML & Rosenbaum DS (2003). Repolarization alternans: implications for the mechanism and prevention of sudden cardiac death. *Cardiovasc Res* **57**, 599–614.
- Wang L, Myles RC, De Jesus NM, Ohlendorf AK, Bers DM & Ripplinger CM (2014). Optical mapping of sarcoplasmic reticulum Ca²⁺ in the intact heart: ryanodine receptor refractoriness during alternans and fibrillation. *Circ Res* **114**, 1410–1421.
- Weiss JN, Karma A, Shiferaw Y, Chen P-S, Garfinkel A & Qu Z (2006). From pulsus to pulseless: the saga of cardiac alternans. *Circ Res* **98**, 1244–1253.
- Weiss JN, Nivala M, Garfinkel A & Qu Z (2011). Alternans and arrhythmias: from cell to heart. *Circ Res* **108**, 98–112.
- Wilson LD, Wan X & Rosenbaum DS (2006). Cellular alternans. *Ann N Y Acad Sci* **1080**, 216–234.
- Xie F, Qu Z, Yang J, Baher A, Weiss JN & Garfinkel A (2004). A simulation study of the effects of cardiac anatomy in ventricular fibrillation. *J Clin Invest* **113**, 686–693.
- Xu Y, Dong PH, Zhang Z, Ahmmed GU & Chiamvimonvat N (2002). Presence of a calcium-activated chloride current in mouse ventricular myocytes. *Am J Physiol Heart Circ Physiol* **283**, H302–H314.
- Xu Y, Tuteja D, Zhang Z, Xu D, Zhang Y, Rodriguez J, Nie L, Tuxson HR, Young JN, Glatter KA, Vázquez AE, Yamoah EN & Chiamvimonvat N (2003). Molecular identification and functional roles of a Ca²⁺-activated K⁺ channel in human and mouse hearts. *J Biol Chem* **278**, 49085–49094.
- Yu C-C, Corr C, Shen C, Shelton R, Yadava M, Rhea IB, Straka S, Fishbein MC, Chen Z, Lin S-F, Lopshire JC & Chen P-S (2015). Small conductance calcium-activated potassium current is important in transmural repolarization of failing human ventricles. *Circulation* **8**, 667–676.
- Zhang Q, Timofeyev V, Lu L, Li N, Singapur A, Long MK, Bond CT, Adelman JP & Chiamvimonvat N (2008). Functional roles of a Ca²⁺-activated K⁺ channel in atrioventricular nodes. *Circ Res* **102**, 465–471.
- Zhang XD, Lieu DK & Chiamvimonvat N (2015). Small-conductance Ca²⁺-activated K⁺ channels and cardiac arrhythmias. *Heart Rhythm* **12**, 1845–1851.

Additional information

Competing interests

None declared.

Author contributions

All authors contributed ideas and discussion. M.K. and D.S. performed computer simulations and mathematical analysis. All authors wrote the manuscript, approved the final version of the manuscript and agree to be accountable for all aspects of the work. All persons designated as authors qualify for authorship, and all those who qualify for authorship are listed.

Funding

This work was supported by National Institutes of Health grant R00-HL111334, American Heart Association Grant-in-Aid 16GRNT31300018 and Amazon AWS Cloud Credits for Research program (D.S.); R01-HL105242 (D.M.B.); and R01-HL085844 (N.C.).

Translational perspective

Recent experimental studies showed that I_{SK} becomes extremely large in failing hearts. Thus, understanding the role of the SK channel in alternans dynamics is potentially important to develop new drugs and therapies for heart failure. In this study, we investigated the role of Ca²⁺-sensitive K⁺ channels (I_{SK} and I_{Ks}) on V_m and Ca²⁺ dynamics. An increase of Ca²⁺-sensitive K⁺ currents can be responsible for electromechanically discordant alternans and quasiperiodic oscillations at the cellular level and Turing-type spatially discordant alternans in tissue. These results provide theoretical bases to understand and interpret experimental and clinical results.

Supporting information

The following supporting information is available in the online version of this article.

Data S1: Details of the model.